

Supporting Information

Fluorescent crystals and co-crystals of 1,8-naphthalimide derivatives: synthesis, structure determination and photophysical characterization

Fabrizia Grepioni,^{a,} Simone d'Agostino,^{a,*} Dario Braga,^a Alessio Bertocco,^a Luca Catalano,^a*

Barbara Ventura^{b,}*

(a) Dipartimento di Chimica "G. Ciamician", Università di Bologna, Via F. Selmi 2, 40126
Bologna, Italy.

(b) Istituto per la Sintesi Organica e la Fotoreattività (ISOF) – CNR, Via P. Gobetti 101, 40129
Bologna, Italy.

Table of Contents

Crystallographic data for crystalline 4 Form I	Page 3
Superimposition of Form I and Form II molecular structures for crystalline 4	Page 3
Types of dimers observed in crystalline 2-4	Page 4
Types of dimers observed in co-crystals n₂·I2F4	Page 4
XRPD for crystalline 2-4 and co-crystals n₂·I2F4	Page 5
ATR-FTIR spectra of components I2F4, 3 and product 3₂·I2F4	Page 6
ATR-FTIR spectra of components I2F4, 4 and product 4₂·I2F4	Page 6
TGA thermograms for the compounds 2, 3 (Form I and Form II), and 4 (Form II)	Page 7
Traces for the compounds: (a) 2 , (b1) 3 (Form I) , (b2) 3 (Form II) , and (c) 4 (Form II)	Page 8
VT-XRPD patterns for crystalline 3 (Form II)	Page 9
TGA thermograms for the co-crystals n₂·I2F4	Page 9
Absorption and emission spectra of 3 and 4 in solution	Page 10
Luminescence data in toluene glassy matrix at 77 K	Page 11
Fluorescence spectra of 2, 3 and 4 in toluene at 77K	Page 11
Structural detail for crystalline 4₂·I2F4	Page 12

Table S1. Crystallographic data and details of measurements for crystalline **4 Form I**.

	4		
Formula	C ₂₃ H ₂₁ N ₃ O ₂	D _{calc} (g/cm ³)	1.349
fw	371.43	packing coefficient (%) ^a	69.9
Cryst. System	Orthorhombic	accessible void (Å ³) ^a	0
Space group	Pna2 ₁	μ (mm ⁻¹)	0.088
Z	4	Measd reflns	7735
a (Å)	30.652(5)	Indep reflns	3143
b (Å)	5.3082(9)	R ₁ [on F _o ² , I>2σ(I)]	0.0663
c (Å)	11.243(2)	wR ₂ (all data)	0.1116
α (deg)	90		
β (deg)	90		
γ (deg)	90		
V (Å ³)	1829.3(6)		

^aCalculated with Platon; for the accessible void calculation a probe of 1.2 Å³ was employed.

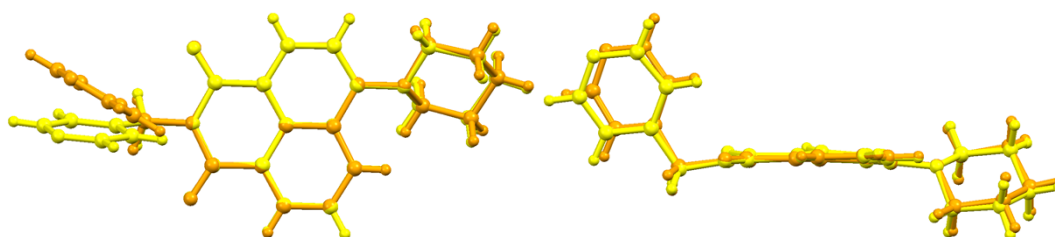


Figure S1. Top (left) and side (right) views for the superimposition of **4 (Form I)** (orange) and **4 (Form II)** (yellow) molecular structures for crystalline **4**, showing that the two conformations are almost exactly the same in the two polymorphs. H_{CH} are omitted for clarity.

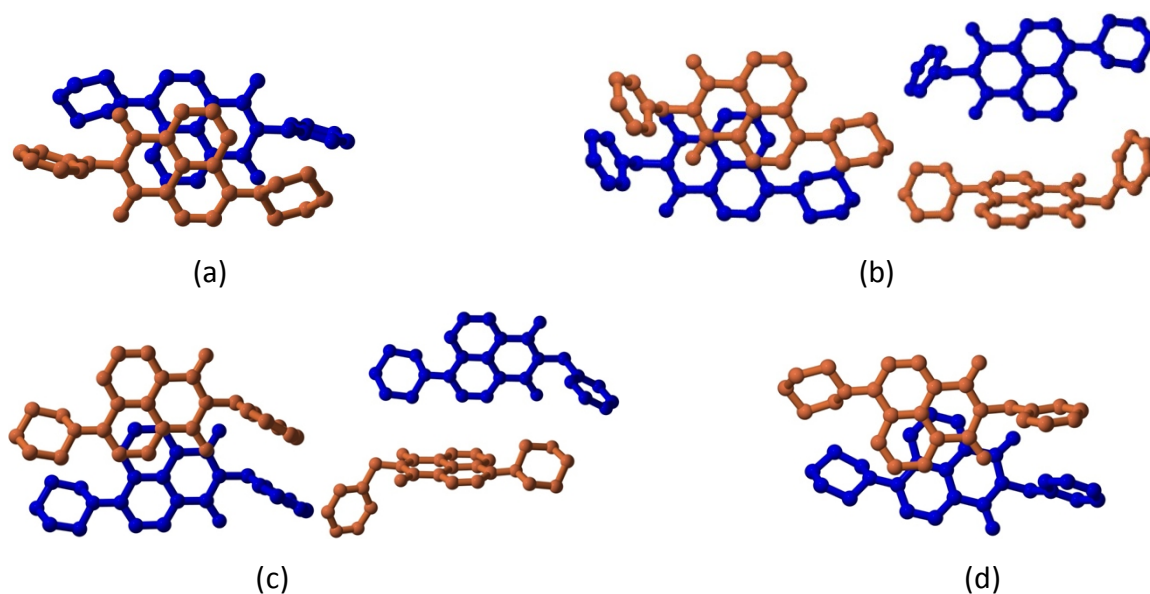


Figure S2. Types of dimers observed in crystalline **2-4**: (a) head-to-tail dimer in crystalline **2**, CD = 3.8Å, ID = 3.4Å, offset = 1.7 Å; (b) head-to-head dimer in crystalline **3**: CD = 5.3 Å, ID = 3.5 Å, offset 3.9 Å (left), and T-dimers with dC–H···π = 3.2 Å or dC···π = 4.0 Å (right); (c) head-to-head dimer in crystalline **4 (Form I)**: CD = 5.3 Å, ID = 3.5 Å, offset 3.9 Å (left), and T-dimers dC–H···π = 2.7–2.9 Å or dC···π = 3.6 Å (right), and (d) head-to-head dimer in crystalline **4 (Form II)**: CD = 4.6 Å, ID = 3.3 Å, offset 3.2 Å. H_{CH} omitted for clarity.

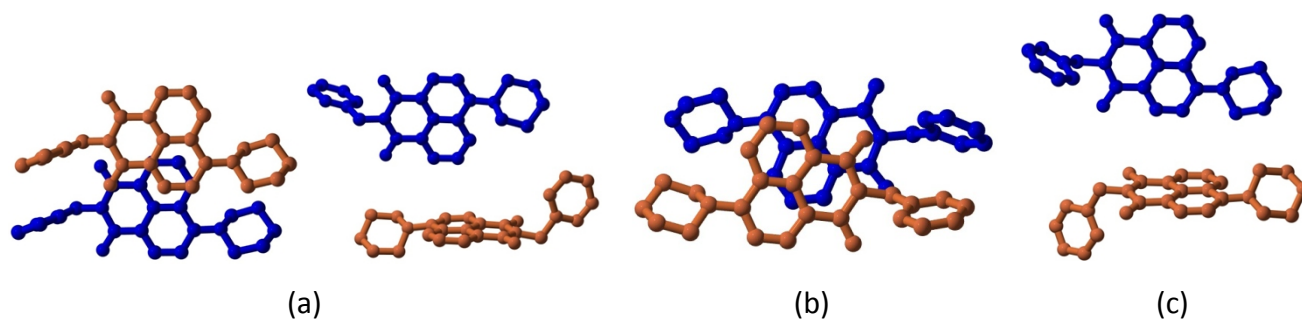


Figure S3. Types of dimers observed in **n₂·12F4** co-crystals. (a) head-to-head dimer in crystalline **2₂·12F4**, CD = 5.2 Å, ID = 3.3 Å, offset = 4.0Å (left), and T-dimer dC–H···π = 2.8–3.1 Å or dC···π = 3.7–3.8 Å (right); (b) head-to-head dimer in crystalline **3₂·12F4**, CD = 4.1 Å, ID = 3.5 Å, offset = 2.1Å; (c) T-dimer in crystalline **4₂·12F4**, dC–H···π = 2.8-3.0 Å or dC···π = 3.7-3.9 Å. H_{CH} omitted for clarity.

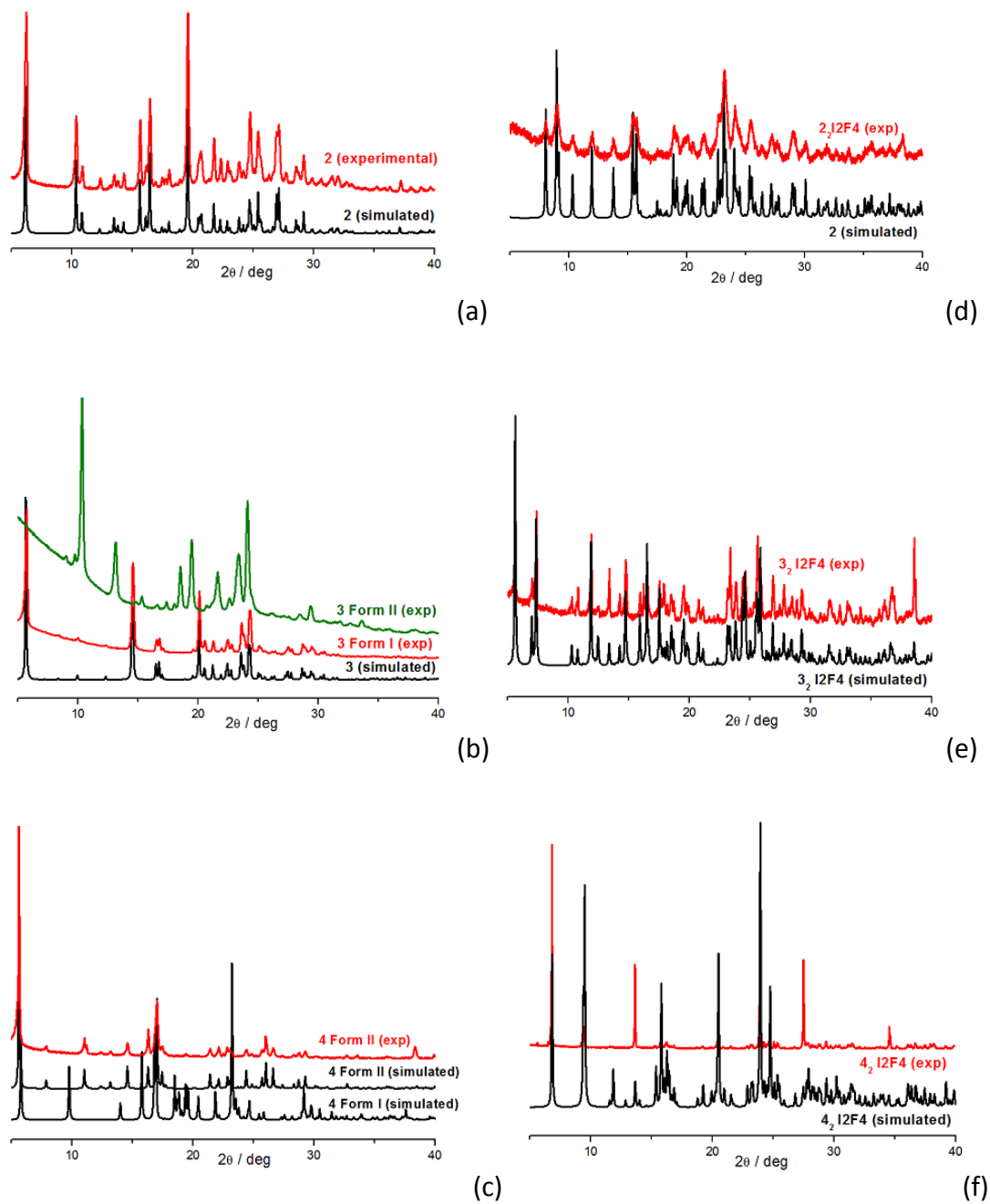


Figure S4. Experimental (red-line) and simulated (black-line) X-ray powder diffraction patterns for compounds: (a) **2**, (b) **3**, and (c) **4** of for corresponding co-crystals: (d) **2₂·12F4**, (e) **3₂·12F4**, and (f) **4₂·12F4**.

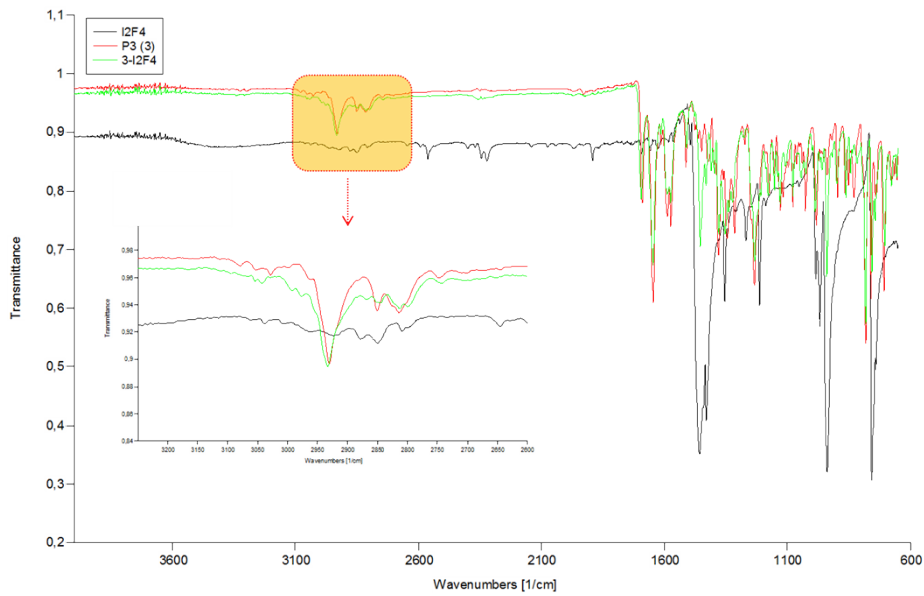


Figure S5. ATR-FTIR spectra of components I2F4 (black line), **3** (red line) and **3**₂·I2F4 (green line) in the range 4000-600 cm⁻¹. The inset highlights the shifts to higher frequencies for the ν_{C_{pyr}-H} stretching (from **3**) of the pyridine involved in the halogen bond.

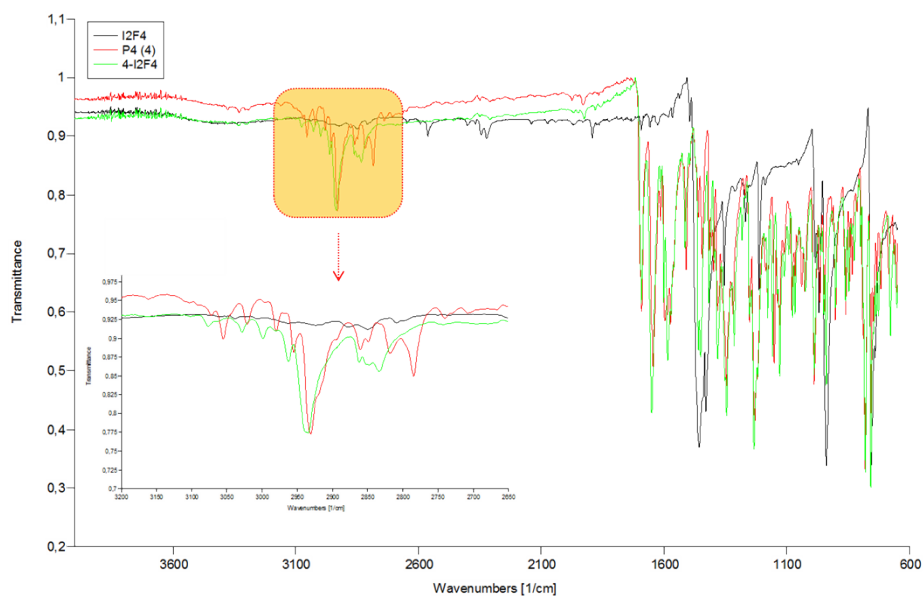


Figure S6. ATR-FTIR spectra of components I2F4 (black line), **4** (red line) and **4**₂·I2F4 (green line) in the range 4000-600 cm⁻¹. The inset highlights the shifts to higher frequencies for the ν_{C_{pyr}-H} stretching (from **4**) of the pyridine involved in the halogen bond.

Thermal characterization (TGA-DSC-VTPXRD).

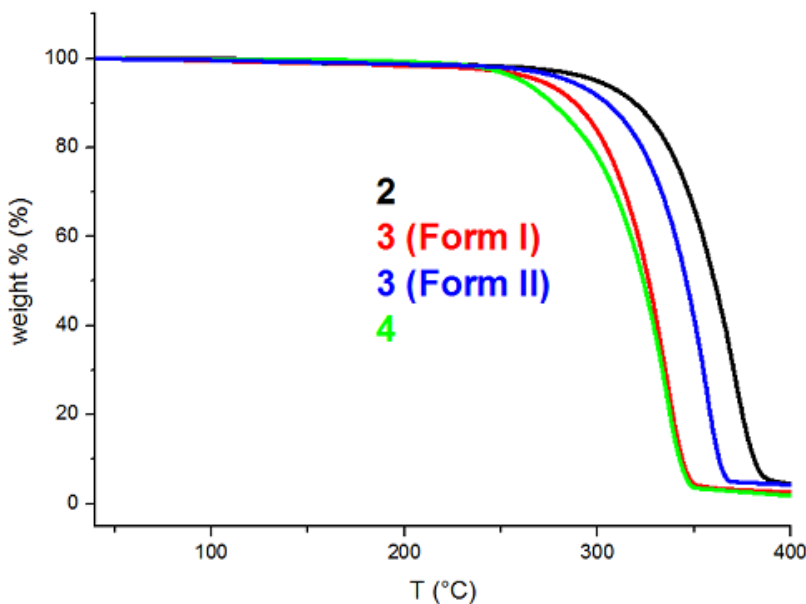


Figure S7. TGA thermograms for the compounds **2**, **3 (Form I and Form II)**, and **4 (Form II)**.

Differential scanning calorimetry (DSC) measurements below the decomposition temperature were also performed, and are shown in SI-Figure 8. For compound **2** the DSC trace shows that melting occurs at ca 190 °C (peak temperature, $\Delta H = 35.8\text{kJ mol}^{-1}$) in the first heating cycle; recrystallization to the same crystalline form is observed in a second heating cycle (exothermic peak at 108 °C, peak temperature, $\Delta H = 17.8\text{kJ mol}^{-1}$), followed by melting at 190 °C (peak temperature, $\Delta H = 35.0\text{kJ mol}^{-1}$) (see SI-Fig. 8). Compound **3 (Form I)** melts at 157 °C (peak temperature, $\Delta H = 28.9\text{kJ mol}^{-1}$) but a second, small peak is observed at ca. 175 °C. Recrystallization occurs during the cooling process and in a second heating cycle, in which melting is observed at 156 °C (peak temperature, $\Delta H = 2.5\text{kJ mol}^{-1}$). When the same measurement is performed on a sample of **3 (Form II)** melting is now observed at 176 °C (peak temperature, $\Delta H = 38.9\text{kJ mol}^{-1}$), and recrystallization occurs on a second heating cycle to **3**

(**Form I**), which melts at 156 °C (peak temperature, $\Delta H = 5.1 \text{ kJ mol}^{-1}$). The small peak observed at 175 °C in the DSC trace of **Form I** is likely due to traces of **Form II**.

The DSC trace of compound **4** (**Form II**) shows an endothermic peak at 181 °C (peak temperature, $\Delta H = 35.9 \text{ kJ mol}^{-1}$), due to melting. A second heating cycle shows the compound melts at the same temperature, i.e. **Form II** recrystallizes from the melt.

The thermal behavior of **3** (**Form II**) has also been investigated via variable temperature X-ray powder diffraction (see SI-Figure 8).

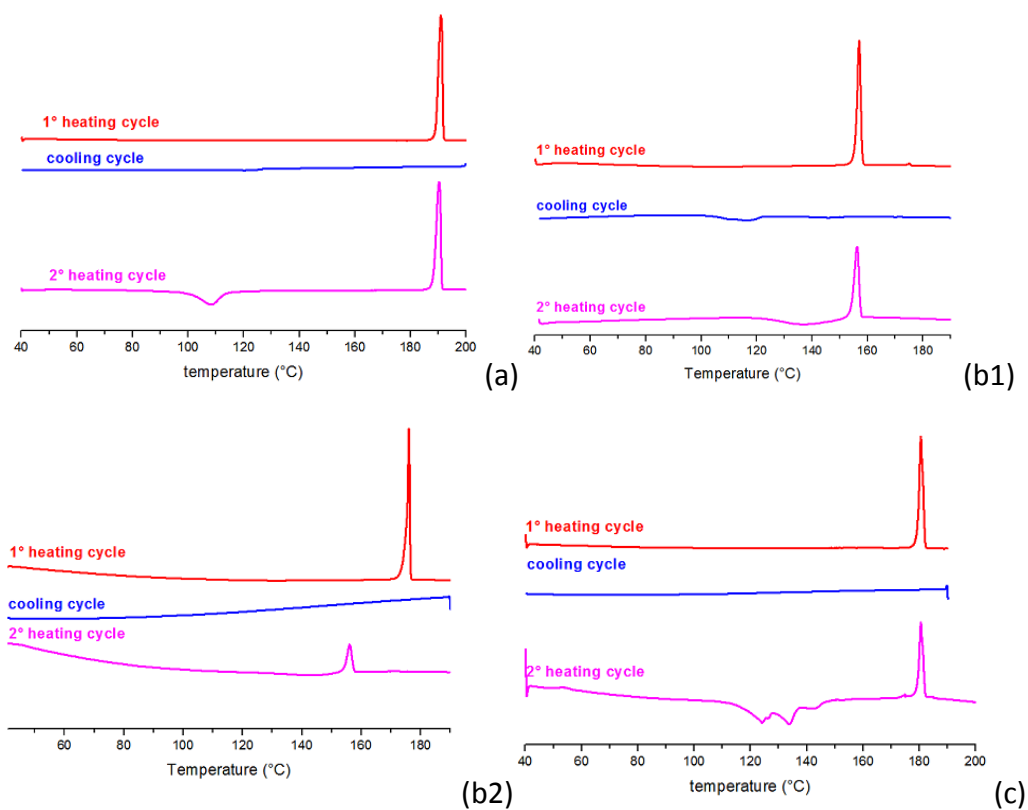


Figure S8. DSC traces for the compounds: (a) **2**, (b1) **3** (**Form I**), (b2) **3** (**Form II**), and (c) **4** (**Form II**).

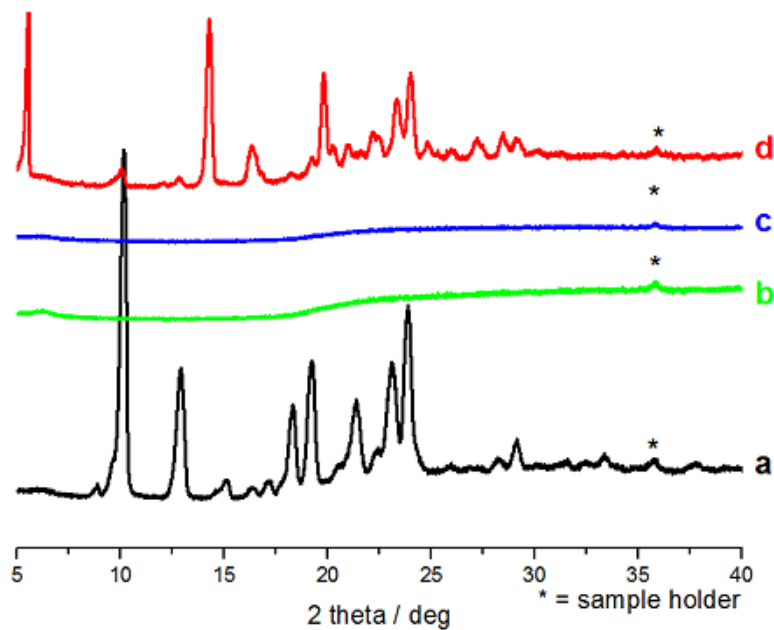


Figure S9. VT-XRPD patterns for crystalline **3 (Form II)** at RT (a), at 180 °C (melting occurs) (b) and back at RT (the solid is amorphous); a second heating to 153 °C (d) shows recrystallization to **3 (Form I)**.

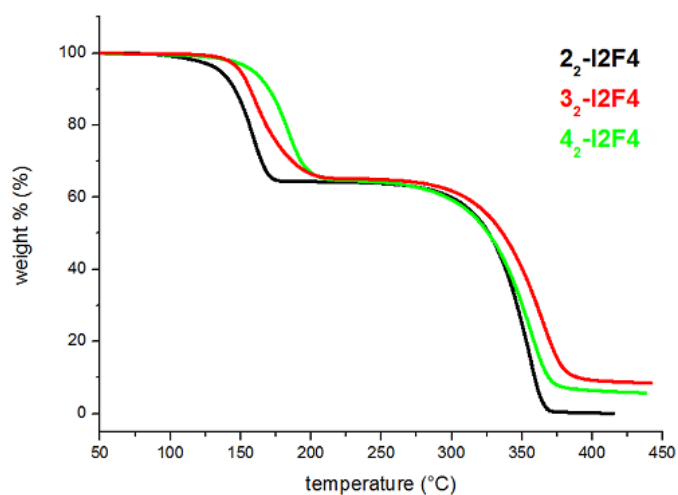


Figure S10. TGA thermograms for the co-crystals **2₂-I2F4**, **3₂-I2F4**, and **4₂-I2F4**.

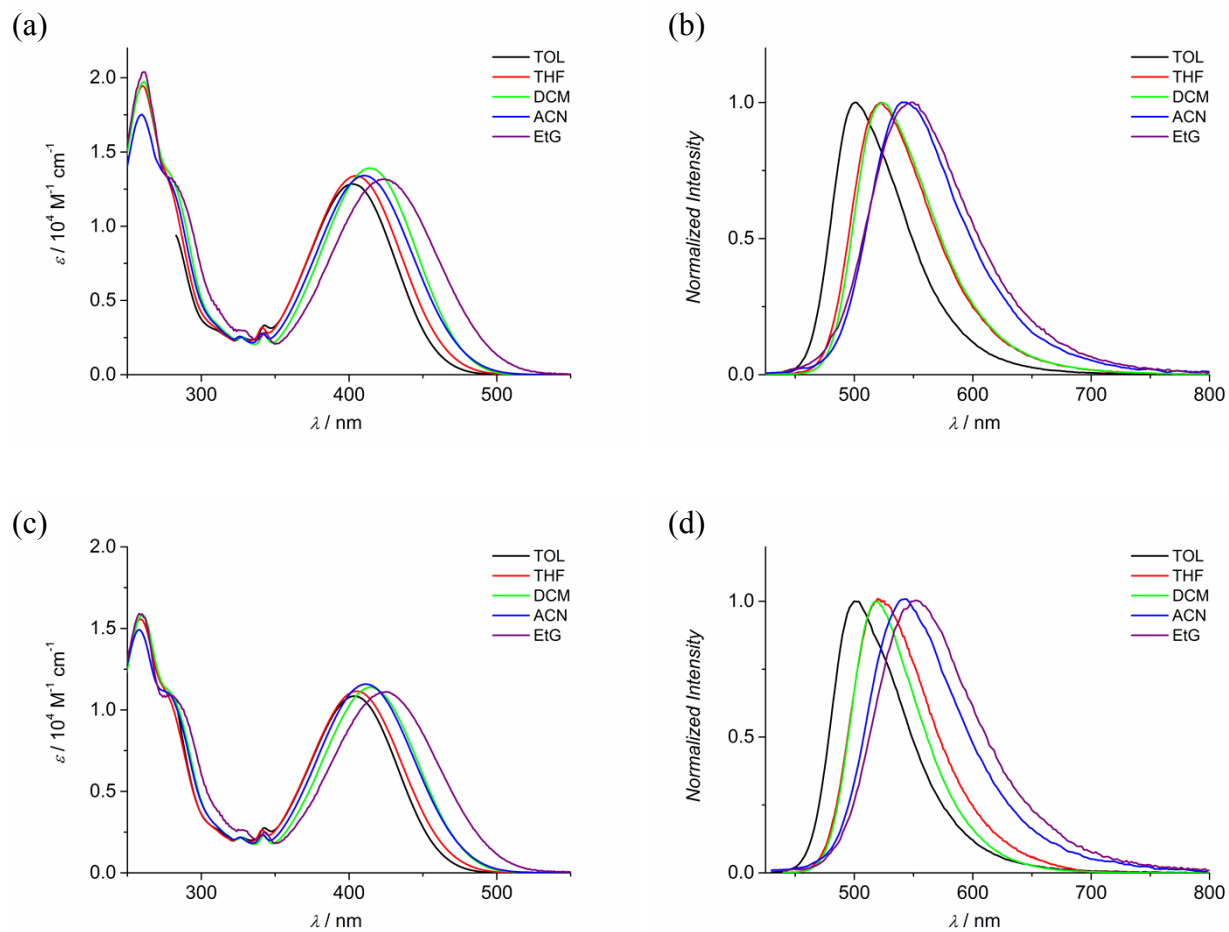


Figure S11. Absorption (a, c) and normalized emission (b, d) spectra of **3** (a, b) and **4** (c, d) in the explored solvents at room temperature.

Table S2. Luminescence data in toluene glassy matrix at 77 K.

	$\lambda_{fl}^{max} / \text{nm}^a$	τ / ns^b	E / eV
2	491	7.0	2.53
3	493	7.2	2.51
4	493	7.1	2.51

^a From corrected spectra. ^bFluorescence lifetimes, excitation at 373 nm.

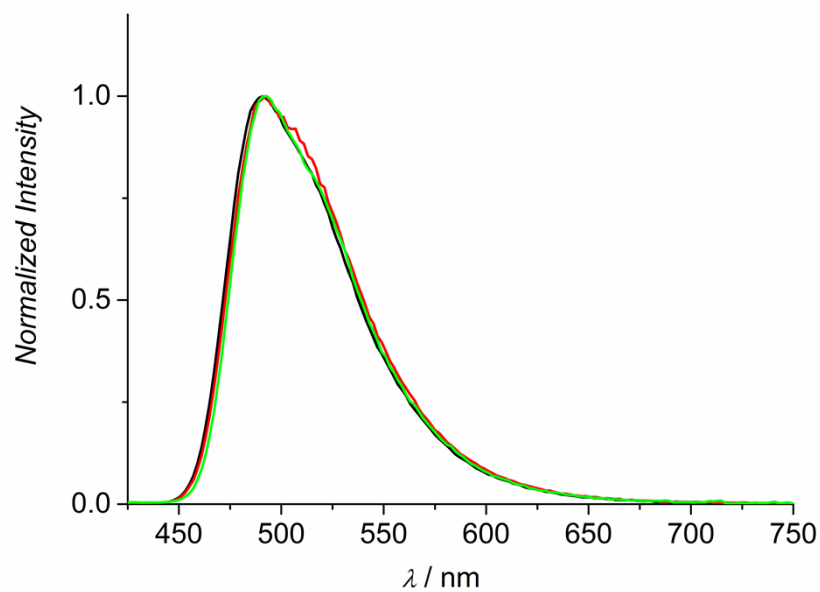


Figure S12. Normalized fluorescence spectra of **2** (black), **3** (red) and **4** (green) in toluene at 77K. Excitation at 400 nm.

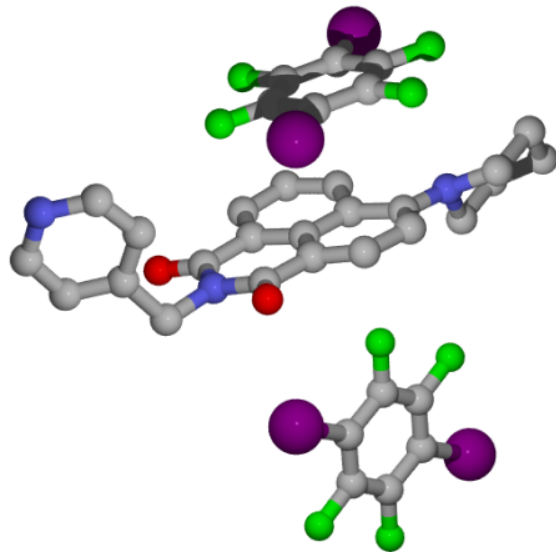


Figure S13. Structural detail that highlights how the halogenated co-formers lie above and below the naphthalimide units in crystalline **4₂·I2F4**. H_{CH} omitted for clarity.